Available online at www.sciencedirect.com
SCIENCE DIRECT
Polymer 46 (2005) 3616–3627
polymer
www.elsevier.com/locate/polymer

# Structure–property relations of segmented block copolymers with liquid–liquid demixed morphologies

Martijn van der Schuur[a,1], Evert van der Heide[b], Jan Feijen[a], Reinoud J. Gaymans[a,*]

[a]*Department of Science and Technology, University of Twente, P.O. Box 217, 7500 AE Enschede, The Netherlands*
[b]*Shell International Chemicals B.V., Amsterdam, The Netherlands*

Received 13 January 2005; received in revised form 2 March 2005; accepted 4 March 2005
Available online 2 April 2005

**Abstract**

Poly(propylene oxide) based polyether(ester-amide)s (PEEA) with non-crystallisable amide segments were synthesized and their structure–property relations studied. These model segmented block copolymers were used to gain insight in the structure–property relations of block copolymers with liquid–liquid demixed morphologies, also present in segmented polyurethanes. The poly(propylene oxide) used had a molecular weight of 2300 g/mol and was end capped with 20 wt% ethylene oxide. The non-crystallisable amide segments are based on an amorphous polyamide: poly(*m*-xylylene isophthalamide) and the repetitive length ($x$) of the amide segment was varied from 1 to 10. Phase separation in these PEEA's occurred by liquid–liquid demixing when the length ($x$) of the non-crystallisable amide segment was higher than 2 ($x>2$). TEM experiments showed spherical structures at two size scales, 5–10 nm domains (nano-domains) and 30–500 nm domains (sub-micron domains), both dispersed in a polyether matrix. The size and volume fraction of these spherical domains were found to increase with increasing the amide segment length. The modulus of the materials increased moderately with increasing amide segment content (increasing amide segment length $x$). The compression and tensile sets values of these PEEA's were found to decrease with increasing amide segment length, thus these PEEA's behave also more elastic at longer amide contents (thus also at higher modulus). Giving time these liquid–liquid demixed segmented block copolymers recovered completely.


*Keywords:* Poly(propylene oxide); Polyurethane; Polyether(ester-amide)

## 1. Introduction

Segmented block copolymers consisting of alternating mobile and rigid segments belong to the family of thermoplastic elastomers (TPE's) [1]. If these rigid and mobile segments are thermodynamically incompatible then micro-phase separation takes place. Phase separation in these segmented block copolymers may proceed through liquid–liquid demixing [2–4], and also through crystallisation [5,6]. If the mobile segment content is in excess, the rigid segments form hard domains dispersed in an amorphous soft matrix. These hard domains act as physical crosslinks, below their glass transition or melting temperature ($T_g$), giving the block copolymer its specific thermoplastic and elastomeric behavior [7,8].

Liquid–liquid demixing occurs for instance in styrenic block copolymers, such as SBS, SEBS and SIS etc. The morphology of these materials consists of amorphous hard domains in an amorphous soft matrix [1]. According to Leibler [9] a binary polymer system phase separates through liquid–liquid demixing if the product of the Flory–Huggins interaction parameter $\chi$ and the degree of polymerization $N$ exceeds a critical value. Thus, liquid–liquid demixing is favored, if the molecular weight of one or both segments increases. Liquid–liquid demixing is a slow process compared to crystallisation [10] and may proceed in the melt, which is known as melt phasing [11–13].

Crystallisation of rigid segments in block copolymers is possible if the structure of this segment is regular like in most polyether(ester)s, polyester- and polyether(amide)s and segmented polyurethanes [1,14,15]. Segmented polyurethanes, for instance polyether(urethane)s and polyether (urethane-urea)s often phase separate through liquid–liquid

* Corresponding author.
*E-mail addresses:* mvds@oce.nl (M. van der Schuur), r.j.gaymans@utwente.nl (R.J. Gaymans).
[1] Present address: OCE, Venlo, The Netherlands.

0032-3861/$ - see front matter © 2005 Elsevier Ltd. All rights reserved.
doi:10.1016/j.polymer.2005.03.010

demixing and also crystallisation [16,17]. First the rigid segments cluster into domains often followed by partial crystallisation of the already phase separated rigid segments [16–20]. The morphology of these segmented polyurethanes is therefore quite complex as it consists of more than two phases [21–23]. Liquid–liquid demixing in segmented polyurethanes and polyamides occurs easily as the urethane, urea and amide segments are poorly miscible with the polyether segments. Phase separation by liquid–liquid demixing in these systems is induced by increasing the rigid segment length [16].

The phase separated hard domains have two functions: they act as physical crosslinks (network properties) as well as filler particles (reinforcement). The reinforcing effect of spherical filler particles on the (storage) modulus of polymers has been described by the Guth–Smallwood relation (Eq. (1)) [24,25]:

$$G = G_{\mathrm{m}}(1 + 2.5\phi_{\mathrm{h}} + 14.1\phi_{\mathrm{h}}^2) \quad (1)$$

In this study the $G$ refers to the storage modulus of the segmented block copolymers, $G_{\mathrm{m}}$ is the storage modulus of the matrix phase (soft phase) and $\phi_{\mathrm{h}}$ is the volume fraction of the hard domains. Eq. (1) holds for polymer systems filled with spherical particles (content $\leq$30 vol%), of which the modulus of the filler is very large compared to the modulus of the soft phase [24,25]. Other relationships describing an increase in the modulus with increasing filler content are those of Kerner, Lewis–Nielsen, Fedors and Landers, Davies and Mooney [26].

Segmented polyurethanes easily degrade at high temperature, which complicates studies on these block copolymers. Segmented polyamides have somewhat similar hydrogen bonding and are more thermally stable. Moreover, there is a wide variety of monomers for amides available and there are less side reactions involved in the synthesis of segmented polyether(ester-amides) (PEEA). Therefore, PEEA are chosen as model block copolymers to study the structure–property relations of liquid–liquid demixed block copolymers. In order to do so, crystallisation in these block copolymers should be absent. Hence, the segmented PEEA's used in our study have amide segments with an irregular structure. Crystallisation of these irregular amide segments is expected to be difficult if not even impossible. The rigid amide segments of the polymers studied are based on polyamides synthesized from *m*-xylylene diamine and diphenyl isophthalate, also known as poly(*m*-xylylene isophthalamide) (Fig. 1). High molecular weight poly(*m*-xylylene isophthalamide) is a transparent amorphous polymer with a softening temperature of 215–225 °C [27]. The amide segment structure resembles that of toluene diisocyanate (TDI) urea segments, so that the results also provide insight in the structure–property relations of segmented polyurethanes. The parameter $x$ in Fig. 1 is the number of amide repeat units, which is an important parameter in this study. The amide segment can be uniform

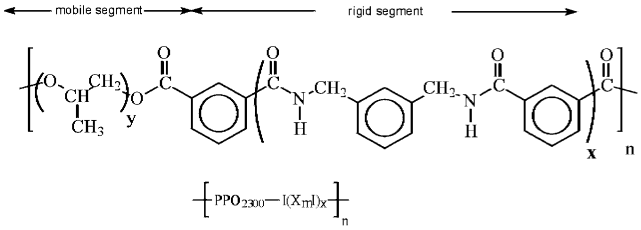


Fig. 1. A PEEA based on poly(propylene oxide) ($PPO_{2300}$) and non-crystallisable rigid segments based on poly(*m*-xylylene isophthalamide). The rigid amide segment length is denoted as $x$, I stands for isophthalamide and $X_m$ for *meta*-xylylene groups.

in length ($x_{\mathrm{u}}$) or can have a random length distribution ($x_{\mathrm{r}}$). To our knowledge, segmented block copolymers with non-crystallisable hard segments of uniform length have not been studied before.

The effect of poly(*m*-xylylene isophthalamide) segment length and segment length distribution in a segmented block copolymers with $PPO_{2300}$ on the phase separation and morphology is studied. In addition, the influence of liquid–liquid demixed amide segments is related to the thermo-mechanical, tensile and elastic properties of the block copolymers.

## 2. Experimental

### 2.1. Materials

Diphenyl isophthalate (DPI), tetra-isopropyl orthotitanate (Ti(*i*-$OC_3H_7)_4$), *m*-xylene, toluene and *N*-methyl-2-pyrrolidone (NMP) were purchased from Aldrich. *m*-Xylylene diamine was a gift from Mitsubishi Gas Chemical Company (Japan). Irganox 1330 was obtained from CIBA. These materials were used as received.

Poly(propylene oxide) end capped with 20 wt% ethylene oxide (EO tipped) (PEO-g-PPO-g-PEO) with a $M_{\mathrm{n}}$ of 2300 g/mol, here further abbreviated as $PPO_{2300}$, was a gift from Bayer AG (Acclaim Polyol PPO-2220 N). Before use, the polyol was dried in vacuum at 80 °C overnight. Osmium tetroxide ($OsO_4$) (4 wt% solution in water) and formaldehyde were purchased from Aldrich.

### 2.2. Synthesis of uniform bisester-oligoamides with amide segment length $x_u$

- $x_{\mathrm{u}}=1$: $IX_mI$-diphenyl was synthesized before (uniformity: 88 mol%, i.e. 88 mol% of the mixture has a segment length of $x_{\mathrm{u}}=1$) [28].
- $x_{\mathrm{u}}=2$: $IX_mIX_mI$-diphenyl was synthesized before (uniformity: 92 mol%) [28].
- $x_{\mathrm{u}}=3$: $IX_mIX_mIX_mI$-diphenyl was synthesized before (uniformity: 79 mol%) [28].

(The uniformity is defined as the mol fraction of segments of the desired length [28]).

### 2.3. Synthesis of polyether(ester-amide)s with uniform amide segments

An example is given in case of a polyether(ester-amide) with uniform tetra-amide segments with length $x_u = 2$. A 250 ml stainless steel reactor equipped with magnetic coupled stirrer (cylindrical flange flask, type cmd 075) was charged with $PPO_{2300}$ (20.0 g, 8.69 mmol), $IX_mIX_mI$-diphenyl (7.39 g, 8.69 mmol), 100 ml NMP and 1 wt% Irganox 1330 (based on PPO) under a nitrogen flow (the magnetic coupled stirring device was important to obtain high vacuum conditions). The reaction mixture was stirred under $N_2$-flow and heated to a temperature of 120 °C in 1 h and maintained for 2 h at 120 °C. The temperature of the reaction mixture was slowly raised to 250 °C in 1 h. The catalyst (2.0 ml, 0.05 M $Ti(OC_3H_7)_4$ in *m*-xylene) was added at 150 °C. At 250 °C, a low vacuum (10–1 mbar, (1000–100 Pa)) was applied for 1 h and finally a high vacuum (0.1–0.08 mbar (10–8 Pa)) for 2 h. Subsequently, the product was cooled to room temperature while maintaining the high vacuum. The polymers were dried in vacuum at 70 °C overnight before use.

### 2.4. Synthesis of polyether(ester-amide)s with random amide segments

An example of the synthesis of a polyether(ester-amide) is given, in case the polymers contains amide segments with an average amide segments length $x_r = 3$. A stainless steel vessel equipped with magnetic coupling stirrer (cylindrical flange flask, type cmd 075) was charged with $PPO_{2300}$ (20.0 g, 8.69 mmol), *m*-xylylene diamine (3.54 g, 26.0 mmol), DPI (11.1 g, 35.0 mmol), 100 ml NMP and 1 wt% Irganox 1330 (based on PPO) under a nitrogen flow. The reaction mixture was stirred under $N_2$-flow to a temperature of 120 °C and kept for 2 h at 120 °C. Hereafter, the temperature was increased in 1 h to 250 °C and maintained for 2 h. The catalyst (2.0 ml, 0.05 M $Ti(OC_3H_7)_4$ in *m*-xylene) was added at 150 °C. At 250 °C a low vacuum (10–1 mbar (1000–100 Pa)) was applied for 1 h and finally high vacuum (0.1–0.08 mbar (10–8 Pa)) for 2 h. In this time the NMP was stripped and the reaction carried out in the melt. After that the melt was cooled to room temperature while maintaining the high vacuum. The polymers were cut out of the reactor and dried under reduced pressure (0.5 mbar (5 Pa)) at 70 °C overnight before use.

### 2.5. Viscometry

Inherent viscosities ($\eta_{inh}$) were measured at a concentration of 0.1 g/dl in phenol/1,1,2,2-tetrachloroethane (1:1 molar mixture) at 25 °C using a capillary Ubbelohde 1B.

### 2.6. $^1H$ NMR

$^1$H NMR spectra of the block copolymers were recorded on a Bruker AC 300 spectrometer at 300 MHz. Deuterated trifluoro acetic acid (TFA-*d*) was used as a solvent. The amide segment length $x$ was calculated from $^1$H NMR spectra and is the ratio of the integral of the peak at 7.4–7.5 ppm ($I_e$) for the four aromatic hydrogens of the xylylene group divided by 2× the integral of the peak at 8.7 ppm ($I_a$) for the two aromatic hydrogens of the isophthatic group on the ester side (Eq. (2)):

$$x = \frac{I_e}{2I_a} \tag{2}$$

### 2.7. Dynamical mechanical thermal analysis (DMTA)

Test samples for DMTA measurements ($70 \times 9 \times 2$ mm$^3$) were prepared on an Arburg H manual injection-molding machine. The test samples were dried in vacuum at 70 °C for 24 h before use. The storage modulus $G'$ and loss modulus $G''$ as function of temperature were measured using a Myrenne ATM3 torsion pendulum at a frequency of 1 Hz and 0.1% strain. The samples were first cooled to −100 °C and then subsequently heated at a rate of 1 °C/min. As the glass transition temperature was taken the temperature at the maximum of the loss modulus. The flow or softening temperature ($T_{flow}$) was defined as the temperature where the storage modulus reached 1.0 MPa. The flex temperature ($T_{flex}$) is defined as the temperature at the start of the rubber plateau region.

### 2.8. DSC

DSC graphs were recorded on a Perkin–Elmer DSC7 apparatus, equipped with a PE7700 computer and TAS-7 software and calibrated with Indium. The test samples were dried in vacuum at 70 °C overnight. The sample (5–10 mg) was heated at a rate of 20 °C/min and the second heating scans were used to determine the transition temperature of the polymer.

### 2.9. Compression set

Samples for compression set experiments were cut from injection-molded bars. The compression set was measured at room temperature according to the ASTM 395 B standard. After 24 h, the compression (25%) was released at room temperature. After relaxation of half an hour, the thickness of the samples was remeasured. The compression set was taken as the average calculated from three measurements. The compression set is defined as (Eq. (3)):

$$\mathrm{CS} = \frac{d_0 - d_2}{d_0 - d_1} \times 100\% \tag{3}$$

with $d_0$, thickness before compression (mm); $d_1$,

compressed thickness (mm); $d_2$, thickness 30 min after release of compression (mm). Compression set as function of time, at room temperature, were also measured.

### 2.10. Transmission electron microscopy (TEM) [29]

A small drop (40 μl) of a 0.3 wt% solution of polymer in hexafluoro isopropanol (HFIP) was cast on a carbon coated copper grid (200 mesh). Subsequently, the grid with polymer film was heated at 20 °C/min to 20 °C above the flow temperature and this temperature was maintained for 10 min. After that, the material was allowed to cool at 3 °C/min to 40 °C below the flow temperature. Annealing at this temperature was conducted for 10 min after which the sample was allowed to cool to room temperature at 3 °C/min (This special heat treatment was necessary to erase any solvent effects generated during casting and to allow crystallisation, if any, in these ultra thin films ($\pm$ 50 nm)). The treated samples were stained with 1 wt% osmium tetroxide/formaldehyde solution for 1 h at 40 °C. TEM measurements were performed on a Phillips CM30 at an accelerating voltage of 300 kV.

### 2.11. Tensile test

The tensile behavior was studied using a Zwick Z020 universal tensile machine equipped with 500N load cell and extensometers on injection-molded bars, cut to dumbbells (ISO 37 s2). Standard tensile test were performed in three-fold according to ISO 37 s3 and the test speed was 50 mm/min (strain rate: $3.33\times10^{-2}\,s^{-1}$). The tensile stress at 10% strain ($\sigma_{10\%}$), the fracture strain ($\varepsilon_{break}$) and fracture stress ($\sigma_{break}$) were determined. All samples were dried in vacuum at 70 °C overnight before testing. The true fracture stress was calculated with Eq. (4):

$$\sigma_{break,true} = \left(\frac{\varepsilon_{break}}{100} + 1\right)\sigma_{break} \tag{4}$$

### 2.12. Tensile set

Cyclic stress–strain experiments were conducted on injection-molded bars cut to dumbbells (ISO 37 s3). A Zwick Z020 universal tensile machine equipped with 500N load cell was used to measure the stress as function of strain of each loading and unloading cycle at a strain rate of $3.33\times10^{-2}\,s^{-1}$ (test speed of 50 mm/min). The strain of each loading–unloading cycle was increased (stair-case loading) and the tensile set if the strain increment was determined as function of the applied strain. The incremental tensile set (TS) was calculated from the following relation (Eq. (5)):

$$\text{Tensile set} = \frac{\Delta\varepsilon_{remining}}{\Delta\varepsilon_{cycle}} = \frac{\varepsilon_{r,cycle(i)} - \varepsilon_{r,cycle(i-1)}}{\Delta\varepsilon_{cycle}}\times 100 \tag{5}$$

With $\varepsilon_{r,\ cycle(i)}$ the remaining strain at the end of cycle $i$ and with $\varepsilon_{r,\ cycle(i-1)}$ the remaining strain at the end of the preceding cycle $i-1$. Direct after the stress was zero a new cycle was started and the strain steps were 10%.

## 3. Results and discussion

Segmented block copolymers based on PPO and amide segments, which are linked together by ester groups, i.e. the so-called polyether(ester-amide)s (PEEA) have been studied (Fig. 1). The amide segments used are based on poly(*m*-xylylene isophthalamide), an amorphous polymer. The amide segment length is varied and at increasing length the amide units become incompatible, and liquid–liquid demixing occurs. The amide segments length has either a random distribution or a uniform size. If the amide segments are of uniform length then on increasing amide segment length a sharp transition from mixing to demixing is expected. The phase separation by liquid–liquid demixing as well as the effect of the liquid–liquid demixed structures on the block copolymer properties is studied.

### 3.1. Amide segments of uniform length

Segmented copolyether(ester-amide)s (PEEA) with uniform amide segments and poly(propylene oxide) with a molecular weight of 2300 g/mol ($PPO_{2300}$) were synthesized (Table 1). The amide segment length ($x_u$) was increased from 1 to 3, i.e. the length of the uniform amide segments increases from diamide to tetra-amide to hexa-amide segments. All block copolymers were synthesized with high molecular weight ($\eta_{inh}$ of 1.3–1.6 dl/g). The uniform length of the amide segments was not affected by *trans*-reactions which can occur during polymerization [28].

At 250 °C, the polymer melt appeared to be transparent for $x_u=1$ and $x_u=2$ and opaque for $x_u=3$. Opacity of the polymer melt with $x_u=3$ suggests that sufficiently large domains are present to scatter light, i.e. melt phasing has occurred. Transparent melts of PEEA's with uniform diamide ($x_u=1$) and tetra-amide ($x_u=2$) segments were observed before [11,13,30]. At room temperature the polymers with uniform diamide ($x_u=1$) and tetra-amide ($x_u=2$) segments are viscous transparent liquids. This suggests that the uniform amide units with $x_u$ 1 and 2 had not phase separated. The polymer with uniform hexa-amide segments ($x_u=3$) was at room temperature an opaque solid, which indicate the presence of phase separated amide domains that provide the dimensional stability.

The critical amid segment length ($x_c$) at which liquid–

Table 1
Properties of PEEA's based on $PPO_{2300}$ with non-crystallisable amide segments with uniform and random length distribution

| | $x^a$ (exp.) | $x^a$ (NMR) | $I(X_mI)_x$ (wt%) | $I(X_mI)_x$ (vol%)[b] | Phys state[c] | $\eta_{inh}$ (dl/g) | $T_{g,soft}$ (°C) | $T_{flex}$ (°C) | $T_{flow}$ (°C) | $G'_{25\ °C}$[d] (MPa) | CS[e] (%) |
|---|---|---|---|---|---|---|---|---|---|---|---|
| **Uniform** | $x_u$ | | | | | | | | | | |
| $I(X_mI)_1$ | 1 | – | 11.2 | – | L | 1.4 | – | – | – | – | – |
| $I(X_mI)_2$ | 2 | 2.2. | 21.1 | – | L | 1.3 | – | – | – | – | – |
| $I(X_mI)_3$ | 3 | – | 26.9 | 23.0 | S | 1.6 | −53 | −30 | 60 | 1.4 | 71 |
| **Random** | $x_r$ | $x_r$ | | | | | | | | | |
| $I(X_mI)_1$ | 1 | – | – | – | L | – | – | – | – | – | – |
| $I(X_mI)_2$ | 2 | – | – | – | L | – | – | – | – | – | – |
| $I(X_mI)_{2.5}$ | 2.5 | 2.6 | 22.9 | 19.3 | S | 1.43 | −53 | −25 | 130 | 1.9 | 60 |
| $I(X_mI)_3$ | 3 | 3.3 | 27.5 | 23.3 | S | 1.62 | −55 | −20 | 120 | 3.7 | 50 |
| $I(X_mI)_4$ | 4 | 5.0 | 36.8 | 32.0 | S | 0.43 | −52 | −30 | 127 | 5.5 | 50 |
| $I(X_mI)_5$ | 5 | 5.6 | 39.7 | 34.7 | S | 0.53 | −50 | −25 | 110 | 5.6 | 44 |
| $I(X_mI)_6$ | 6 | 6.4 | 43.3 | 39.7 | S | 1.19 | −51 | −35 | 175 | 12 | 12 |
| $I(X_mI)_8$ | 8 | 9.3 | 52.5 | 46.4 | S | 0.87 | −52 | −35 | 177 | 21 | 23 |
| $I(X_mI)_{10}$ | 10 | 10.6 | 54.8 | 47.7 | S | 0.66 | −35 | −35 | 195 | 47 | 17 |

[a] Amide segment length = $x$; uniform length distribution: $x_u$ and random length distribution: $x_r$.
[b] Calculated volume content (based on wt% amide and density of both phases: 1.0 g/cm$^3$ (polyether) and 1.2 g/cm$^3$ (amide phase)).
[c] Physical state at room temperature (L = (viscous) liquid, S = solid/rubber).
[d] Storage modulus at 25 °C.
[e] Compression set at 25 °C.

liquid demixing occurs in PEEA's with $PPO_{2300}$, is $x_c = 3$ and the phase-separated structures appear to be present already in the melt of the block copolymers. Koberstein et al. [31] found for the urethane segment a critical average segment length of 3.3. Above this critical length phase separated urethane segments were present, while below this critical length the urethane segments remain dissolved.

### *3.1.1. Morphology of block copolymers with uniform amide segments*

TEM experiments were performed on ultra-thin films of PEEA's prepared by a solvent casting technique as described by Lothmar et al. [29]. These authors reported no significant differences between the TEM images of samples prepared by the solvent casting technique and by cryo ultra-microtomy.

In the TEM image of the PEEA with a uniform non-crystallisable hexa-amide segments ($x_u = 3$) a dispersion of spherical particles is observed (Fig. 2) (Table 2). The largest spherical domains have a diameter of approximately 150 nm (sub-micron domains) and also many smaller domains (nano-domains) are visible (Fig. 2(b)). The size of the nano domains consisting just of amide segments is expected to be 3 nm, based on the extended length of 6 nm with a random coil structure [3]. The fraction of sub-micron domains observed by TEM is about 8 vol%.

The ~100 nm sub-micron domains are much larger in diameter than the amide segment length, which for $x = 3$ is 5 nm. For ~100 nm domains the length of the chains in these sub-micron domains is expected to be about 200 nm. Chains with a length of 200 nm contain both amide and PPO segments and thus the sub-micron domains contain both amide and PPO segments. The detailed TEM micrograph (Fig. 2(b)) suggests that sub-micron domains do not seem to be homogeneous. The PPO segments in these sub-micron domains must be phase separated due to the incompatibility of PPO segments with the amide phase. A cartoon is drawn for the possible structures (Fig. 3). Fig. 3(a) represents the morphology of block copolymers with short dissolved amide segments with a length of $x \leq 2$. In Fig. 3(b), the polyether phase (A) contain demixed the amide segments (B). The phase separation is both in nano particle that just contain amide segments and sub micron 'salami type' particles with a continuous amide phase and a dispersed ether phase. This liquid–liquid demixed in morphology is present in PEEA copolymers if the amide segment length is 3 or longer ($x \geq 3$).

In order to estimate the amount of amide in the nano particles the amount of amide in the sub-micron particles

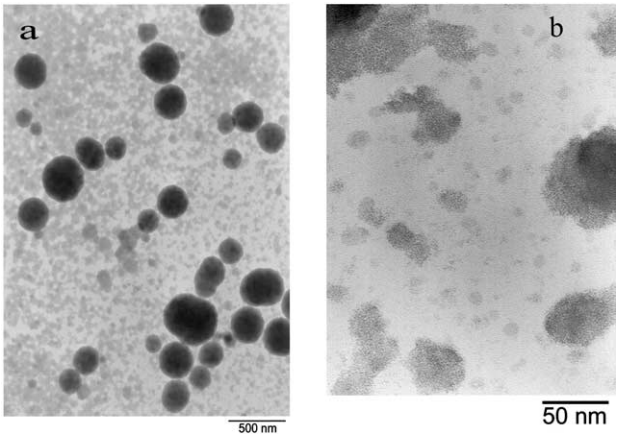


Fig. 2. TEM image of a PEEA with uniform non-crystallisable hexa-amide segment ($x_u = 3$, 23 vol%) stained with 1 wt% $OsO_4$/formaldehyde solution: (a) 52,000×; (b) 120,000×.

Table 2
Composition of liquid–liquid demixed PEEA segmented block copolymers

| | | $x_u=10$ | $x_r=3$ | $x_r=10$ |
|---|---|---|---|---|
| Block copolymer | Amide content (wt%) | 26.9 | 27.5 | 54.8 |
| | Amide content (vol%) | 23 | 24 | 48 |
| Sub-micron particles | Size (nm) | 30–200 | 50–500 | 50–1000 |
| | Content (vol%) | 8 | 13 | 40 |
| | Amide content (vol%) | 2 | 3 | 19.2 |
| Nano-particles | Size (nm) | 3 | 2–10 | 4–20 |
| | content (vol%) | 17 | 16 | 15 |
| Dissolved amide segments | (vol%) | 4 | 4 | 6 |
| Total particle content | (vol%) | 24 | 29 | 55 |

and the dissolved amount of amide segments in the PPO phase has to be determined (Table 2).

Rod-like or co-continues structures were not observed. This is probably due to the process of phase separation during polymerization as in segmented polyurethanes and ABS [16,32]. The amide concentration in the sub-micron particles is assumed to be the same as in the polymer (26.9 wt%, 23 vol%). In that case 8 vol% of sub-micron particles contains about 2 vol% amide. The amount of amide dissolved was obtained from the $T_g$-shift and the 5 °C (Section 3.4.2) corresponds to about 4 wt% amide (4 vol%). The amount of amide nano-particles present is than about 17 vol%, which is a considerable amount.

### 3.2. Amide segments of random length

PEEA's with non-crystallisable amide segments with a random length distribution were also synthesized with relatively high inherent viscosities (Table 1). The average amide segment length ($x_r$) ranged from $x_r=1$–10. The melts of all these copolymers were opaque during polycondensation at 250 °C, even for the copolymers with an average length of $x_r=1$ and $x_r=2$. At a random amide segment length of 2.5 and more, the copolymers were solid at room temperature. The average amide segment lengths as calculated from the amide:ester ratios from $^1$H NMR experiments are somewhat higher than expected [28]. In the one-pot synthesis, which is the process to obtain block copolymers with random amide segments, some of the diphenyl isophthalate may be completely converted by the reaction with PPO thereby extending the PPO segments.

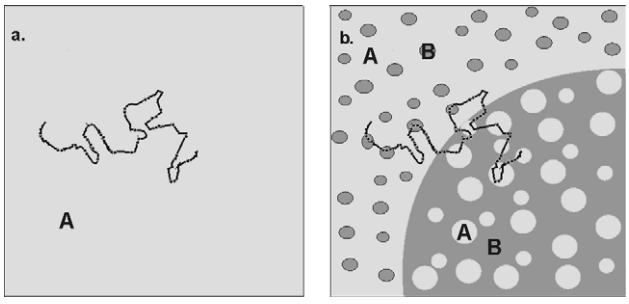


Fig. 3. Cartoon of the morphology of PEEA's with non-crystallisable amide segments and $PPO_{2300}$: (a) short amide segments dissolved; (b) phase separated amide segments with phase A is polyether phase and phase B is the phase separated amorphous amide phase.

#### 3.2.1. Morphology of block copolymers with amide segments of random length

The morphologies as examined by TEM of the polymers with random amide segment lengths $x_r=3$ and $x_r=10$ are shown in Fig. 4(a) and (b), respectively.

The morphology of the PEEA with random amide segment length $x_r=3$ (Fig. 4(a)) consists of a dispersion of spherical sub-micron domains with diameters of approximately 50–500 nm (appr. 13 vol%) and many nano-domains (Table 2). The nano-domains are expected to contain only amide segments and the nano-particle size is therefore a function of the amide segment length. With an amide segment length of 6 nm the size of the particles is expected to be on average 3 nm (2–10 nm). The sub-micron domains are much larger than the amide segment length and must contain PPO segments as well, with a composition similar to that of the copolymer (27.5 wt% amide or 23.5 vol%). The 13 vol% sub-micron particles then contain ~3 vol% amide. Furthermore, part of the amide segments ($x=2$) may be mixed with the PPO phase (~4%). The estimated amount of amide in the nano-particles is 16 vol%.

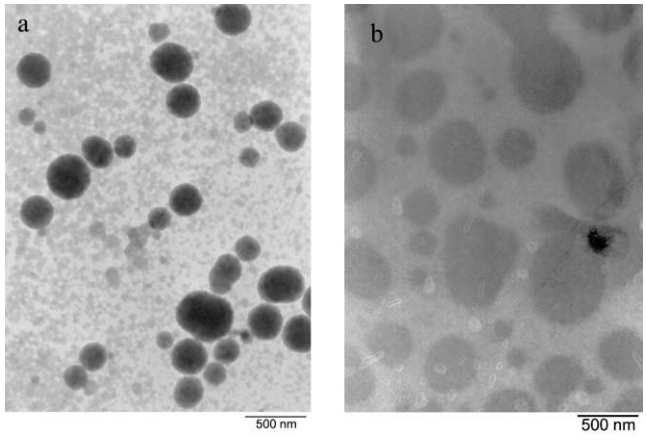


Fig. 4. TEM images (21,000×) of a PEEA with random non-crystallisable amide segments and $PPO_{2300}$ stained with 1 wt% $OsO_4$/formaldehyde solution: (a) average amide length $x_r=3$ (23 vol% amide); (b) average amide length $x_r=10$ (48 vol% amide).

The PEEA with a random amide segment length of $x_r = 10$ (Fig. 4(b)) has a morphology containing spherical sub-micron domains of approximately 50–1000 nm and many nano-domains. The nano-domains with $x_r = 10$ are expected to have an average diameter of 9 nm (5–20 nm) (Table 2). No co-continues structures were observed which is unusual for block copolymer containing 55 wt% of amide segments (48 vol% amide phase). The amount of domains visible (> 50 nm) in the TEM images is ± 40 vol% (19.2 vol% amide). Next to that are amide segments dissolved ($x = 2$) in the PPO phase (~6 wt%). The estimated amount of nano-domains is ~15 vol% (Table 2). Thus, increasing the amide segment length from $x_r$ is 3 to 10 results in larger sub-micron particles and larger nano-particles but the volume fraction of nano-particles is hardly changed.

### 3.3. Hard domain size distributions

The observed morphology of liquid–liquid demixed amide segments is a combination of dispersed spherical nano- and sub-micron domains (Fig. 3(b)). From these TEM-images the sub-micron domain size distribution was determined (Fig. 5). Below 50 nm (nano-domains), it was not possible to measure the size and concentration of the nano-particles well and estimated values are given as a dashed line. When uniform amide segments with $x_u = 3$ are employed the liquid–liquid demixed morphology of the corresponding PEEA shows a bimodal size distribution of spherical nano-domains (±3 nm) and sub-micron domains of 30–200 nm (Fig. 5(a)). With random amide segments compared to uniform length amide segments more of the larger domains are present and also the size of these sub-micron domains is higher.

At longer amide segment length ($x$ 3–10) both the nano and the sub-micron particle sizes increases (Fig. 5(b)). Also the relative content of the larger sizes increases. The PEEA's studied have a bimodal distribution of nano particles (2–10 nm) and sub-micron particles (30–300 nm). For PEUU from TDI and PPO, similar size scales of urea hard domains were detected in by Neff et al. [32].

The large spherical domains are built from long chains and thus contain both amide and PPO segments. In these spherical domains are the amide segments the continuous phase and the PPO the dispersed phase (Fig. 3(b)). Examination of TEM images of the PEEA with $x_r = 10$, at higher magnifications, seems to support this inverted phase morphology of the dispersed phase. Such 'salami type' morphologies are often seen in HIPS and ABS materials [33]. The concentration of amide segments in these large domains increases with amide segment length (Table 2).

### 3.4. Properties of liquid–liquid demixed segmented block copolymers

#### 3.4.1. Thermal properties by DSC

Melting endotherms were not observed in the DSC curves of the block copolymers. This suggests that the amide segments are fully amorphous. Glass transition temperatures of the amide phase were occasionally detected by DSC if the amide concentration was high (>39 wt%). A glass transition temperature of 119 °C is observed for a polymer with 39.7 wt% amide (high amide segment length), which is in good agreement with a flow temperature of 110 °C as measured by DMTA (Table 1).

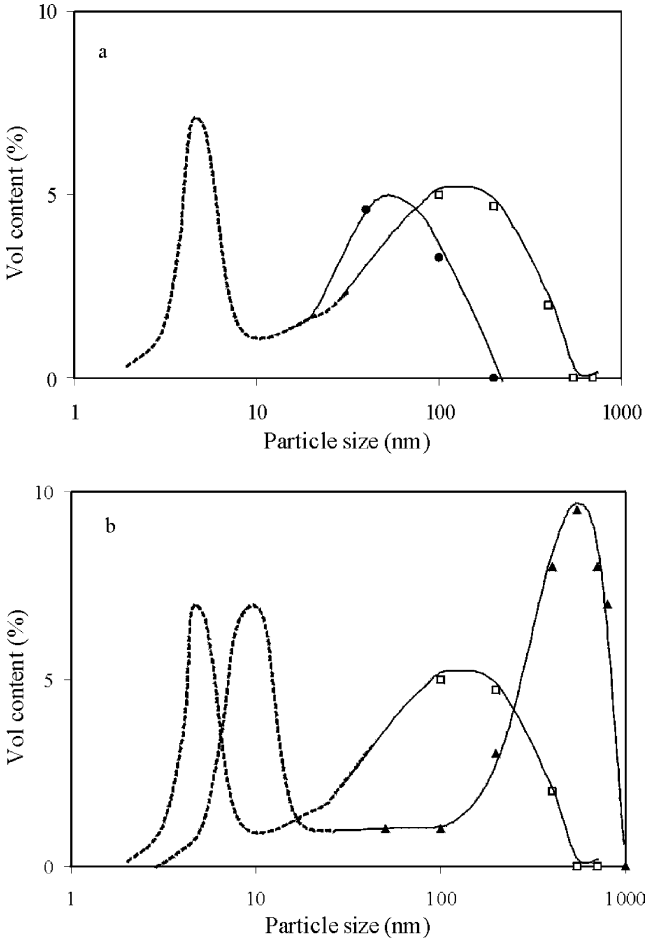


Fig. 5. Domain size distributions of PEEA's with non-crystallisable amide and $PPO_{2300}$ segments. (a) $x = 3$: ■, uniform; □, random (b) □, random $x = 3$; ▲, random $x = 10$ (dashed line: is estimated distribution of nano-domains).

#### 3.4.2. Thermo-mechanical properties by DMTA

The storage and loss modulus of PEEA's with random amide segment length $x_r$ ranging from $x = 3$–10 and $PPO_{2300}$ were measured as function of temperature (Fig. 6). The $G''$ for $x = 8$ is left out for clarity. The storage modulus of the rubber plateau and the flow temperature increases with amide segment length. Two transitions can be seen, a $T_g$ of the polyether phase and a $T_{flow}$ of the amide phase, which indicates that the polymers have a two-phase structure.

The glass transition temperature of the $PPO_{2300}$ phase is sharp and at about −52 °C (Table 1 and Fig. 6(B)). The effect of the amide content and amide length is thus

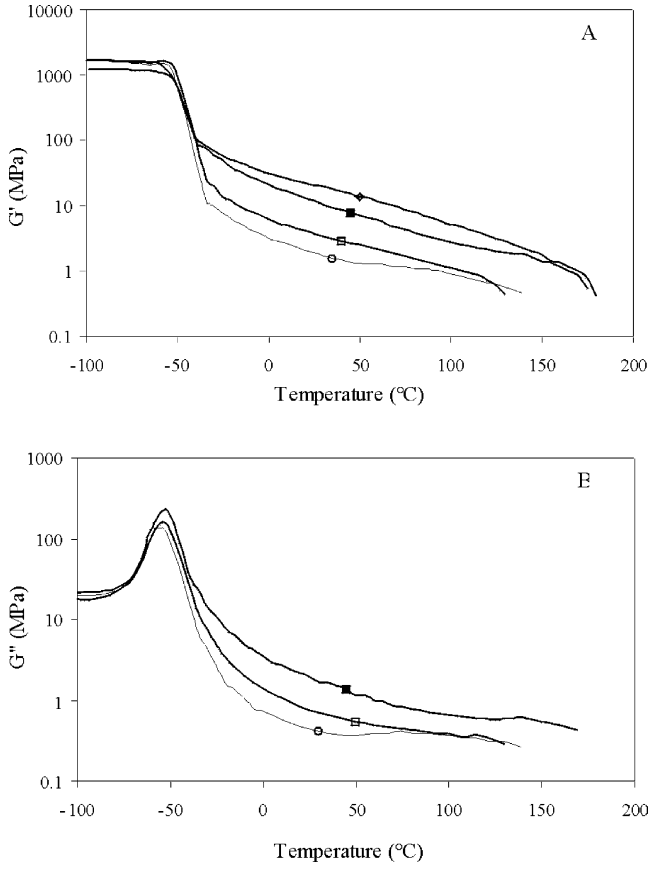


Fig. 6. Storage ($G'$) (A) and loss modulus ($G''$) (B) as function of temperature of PEEA's with non-crystallisable amide segments with different random amide segment length $x_r$: ○, 2.5 (22.9 wt%); □, 4 (36.8 wt%); ■, 6 (43.3 wt%); ♦, 8 (52.5 wt%).

minimal. The higher $T_g$ of the soft phase with regard to the $T_g$ of pure PPO (−75 °C) is probably due to the 'crosslinking' of the $PPO_{2300}$ segments [34], and may also be due to the fraction of dissolved amide segments [3]. The effect crosslinking on the $T_g$ can be described with Eq. (6) [2].

$$T_g = T_g^{\infty} + \frac{3.9 \times 10^4}{M_c} \quad (6)$$

With $T_g$ the glass transition temperature of the segmented block polymer and $T_g^{\infty}$ the glass transition temperature of the soft segment at infinitive molecular weight ($T_g$ of PPO incl 20% EO is −74 °C [14] and $M_c$ is the length between crosslinks. $M_c$ is for PPO with a $M_n$ of 2300 is 2300 g/mol. On the basis of this is the $T_g$ of the $PPO_{2300}$ in between crosslinks and without amide dissolved is −57 °C.

The $T_g$ shift as a result of dissolved amide segments is thus about 5 °C (−57 to −52°). With the Fox relationship and taking for the $T_g$ of the poly(*m*-xylylene isophthalamide) 225 °C the concentration of dissolved amide is 4 wt%.

The flex temperature of these liquid–liquid demixed block copolymers is at approximately −30 °C (=$T_g$+20 °C) indicating an excellent low-temperature flexibility of these PEEA's due to the use of poly(propylene oxide) segments.

The modulus ($G'$) of the copolymers decreases with temperature and also increases with increasing amide content. The increase in the modulus with amide content is expected to be due to the reinforcing effect of the phase separated amide domains. Such a reinforcing effect can be described by the Guth–Smallwood relation (Eq. (1)). The increase in modulus is given as function of the hard segment content (Fig. 7).

The hard segment content can be either the amide content or the particle content. The particle content is higher than the amide content as the sub-micron 'salami type' particles also contain PPO segments (Fig. 3(b)). Increasing hard content by increasing the amide content, results in a linear increase with the logarithm of the storage modulus (Fig. 7, closed symbols). This increase is stronger than predicted by the Guth–Smallwood relation (Eq. (1)), hereby it is assumed that the modulus of the spherical hard domains (the reinforcing polyamide phase) is at least 1000× the modulus of the soft matrix (the polyether phase). In the case of PEEA's with uniform hexa-amide segments ($x_u$=3) the modulus-composition is somewhat closer to the prediction of Guth–Smallwood. This polymer contains smaller amounts of the large spherical domains than the polymer having a random amide segment length $x_r$=3 (Fig. 5(a), Table 2).

The particle content is given for a few samples from the TEM images (Table 2) by assuming that the 'salami type' particles have the same overall composition as the whole system. The particle volume content is slightly higher than the amide volume content (Fig. 7, open symbols). The storage modulus of the PEEA's as function of the particle content, i.e. thus also including the polyether phase inside the larger domains, is closer to the relation of Guth–Smallwood. In this approach it was assumed

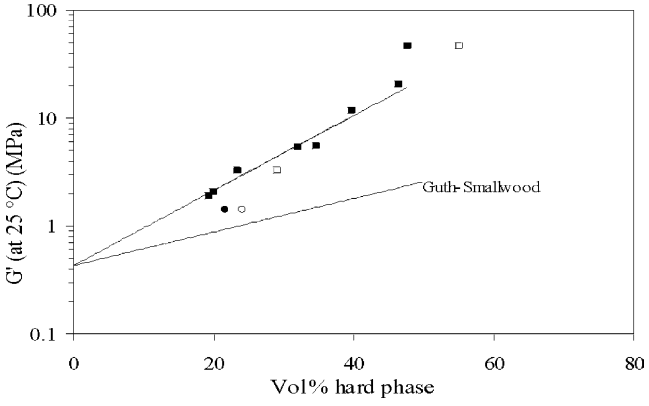


Fig. 7. Storage modulus at 25 °C as function of the hard phase content (vol%): ■, amide content random segments; ●, amide content uniform segment $x_u$=3; □, particle content random segments; ○, particle content uniform amide segment $x_u$=3; (line I represents the Guth–Smallwood relation, Eq. (1)).

that there are no inter-facial layer effects. The idea that the increase in modulus in these block copolymers is due to the filler effect of the spherical particles seems to hold.

### 3.4.3. Elastic behavior by compression set

As a first estimate of the elasticity of the PEEA's, the compression sets at 25% strain are determined (Table 1, Fig. 8). The compression set (CS) at room temperature of the PEEA's decreases with increasing amide segment length $x$ (increasing amide content) and thus increasing modulus. Also remarkable is that the block copolymer with uniform amide segments, have a somewhat higher CS than block copolymer with random amide segments. The effect of decreasing CS with increasing hard segment content is opposite to what has been observed in previous research on segmented polyether(urethane)s [35] and segmented PEEA's [30,36].

Upon deforming a block copolymer sample, most deformation occurs in the soft polyether phase and this deformation is expected to be fully elastic, just as in block copolymer with chemically cross-linked PPO. The non-elastic behavior is thus due to plastic and/or viscoelastic deformation of the amide phase. With increasing amide segment length the size of both the sub-micron and nano-particles increases. Thus, the decrease in CS seems to be due to the increase in particle sizes. The larger particles are apparently more resistant to deformation than the smaller particles.

This also explains the higher CS values of the uniform amide segments as that system has smaller particle sizes and a higher concentration of nano-particles (Fig. 5(a)). As yet it is not clear whether the deformation occurs mainly in the sub-micron or in the nano-particles.

In a standard ASTM CS test the sample is allowed to recover for 30 min (1800 s) before measuring the residual strain. However, little is known of the effect of the time of recovery on the CS of liquid–liquid demixed block copolymers. The CS-values were determined as function of the time of recovery (Fig. 9). Surprisingly in time, the liquid–liquid demixed PEAA with random amide segments recovered completely. With $x_r = 3.3$ the recovery to almost 0% is in 12 days and with $x_r$ is 6.4 and 9.3 even faster (4 and 1.5 days).

Theoretically at time 0 s, the compression set is 100% and the subsequent recovery with time can be divided into more than one time regime: an elastic (instantaneous) and a viscoelastic response. In a semi-logarithmic plot of CS as functions of recovery time, the viscoelastic recovery shows a S-shaped curve (Fig. 9). This viscoelastic recovery is slow for polymers having an average length of 3.3. This is however relatively fast for polymers with average amide segment lengths of 6.4 and 9.3.

As the viscoelastic recovery is a function of the amide length is must be due to the deformation of the amide phase. It is difficult to see how this is possible. The deformation the hard domains depends on the ratio of the moduli of the hard and soft phase as given by Eq. (7) [37]:

$$\varepsilon_{\text{hard}} = \frac{E_{\text{soft}}}{E_{\text{hard}}}\varepsilon_{\text{soft}} \tag{7}$$

with $E_{\text{soft}}$ and $E_{\text{hard}}$ the moduli of respectively the soft and hard phase ($E_{\text{soft}} \approx 1.2$ MPa and $E_{\text{hard}} \approx 2000$ MPa [38]) and the applied strain is mainly $\varepsilon_{\text{soft}}$. At a strain of 25% strain deformation of the hard phase ($\varepsilon_{\text{hard}}$) is expected to be about 0.02%. At a strain of 0.02% the amide phase should behave fully elastic. A possible explantion for the visco elastic effects is than not the whole amide particle is deformed but that individual polymer chains are pulled out off the liquid–liquid demixed particles. The amorphous amide domains have glass transition temperatures well above room temperature and retraction of these polymer chains, after releasing the compressive strain, back into the hard domains may therefore be slow. With longer amide segments the concentration on nano-particles is smaller but also with these larger nano-partiles it might be more difficult to pull a chain out of the amide phase. This may explain why these liquid–liquid demixed PEEA copolymers show a slow

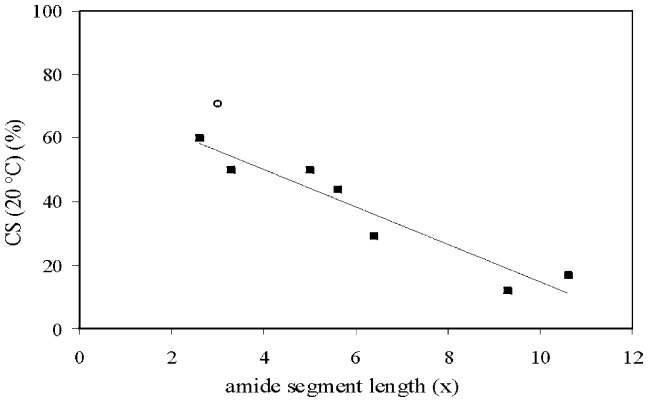


Fig. 8. The compression set at room temperature as function of amide segment length ($x$): ■, random amide segments; ○, uniform amide segment.

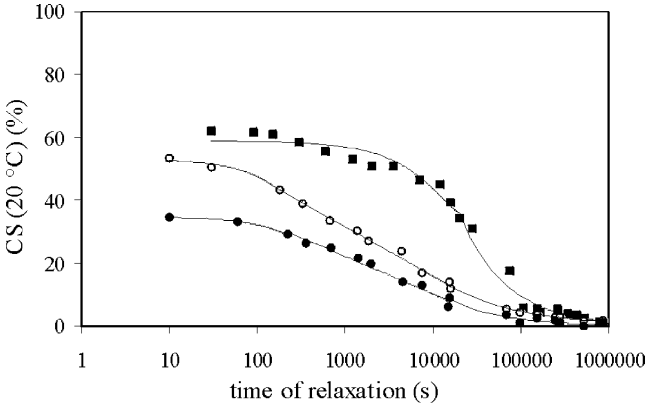


Fig. 9. The compression set as function of relaxation time with random amide segment length $x_r$: ■, 3.3; ○ 6.4; ● 9.3 (dashed line: ASTM 395B standard: 30 min of recovery).

viscoelastic recovery, which decreases with increasing amide length.

### 3.4.4. Stress–strain behavior

On injection molded samples the stress and strain behavior is studied (Table 3).

The tensile stress at 10% strain ($\sigma_{10\%}$) increases with amide segment length, in a similar way as the storage modulus ($G'$). The storage modulus is measured at very low strains (0.1%). The fracture properties look eratic and seem to be more dependant on the molecular weight of the polymer than on the amide segment length (content). The fracture strain decreases with increasing amide segment length ($x$), while the fracture stress increases with increasing amide segment length ($x$). The true fracture stress (Eq. (4)) is a good value for comparing the fracture properties of TPE materials and is plotted as function of the inherent viscosity (Fig. 10).

The true fracture stress increases linearly with inherent viscosity. The fracture properties of these segmented copolymers are thus highly dependant on their molecular weights.

### 3.4.5. Cyclic stress–strain behavior: tensile set

The incremental tensile set (TS) of PEEA's was studied as function of the applied strain (Fig. 11). In the strain region 0–25% the tensile set increases with and levels off after 25% of strain. This plateau may be ascribed to yielding of the amide phase. At higher strains the tensile set increases again. With longer amide segments this last process occurs at lower strains: for $x_r = 10$ at 100% strain and for $x_r = 6$ at 250% strain. The tensile set decreases with increasing amide segment length ($x$) (in the region of 0–100% strain). This surprising result is in line with the lower compression set values obtained for polymers with higher amide segment length $x$ (Fig. 8).

## 4. Conclusions

Polyether(ester-amide)s (PEEA) with non-crystallisable amide segments with high molecular weights were synthesized. These model segmented block copolymers give insight in the structure–property relations of segmented block copolymers with liquid–liquid demixed morphologies such as segmented polyurethanes.

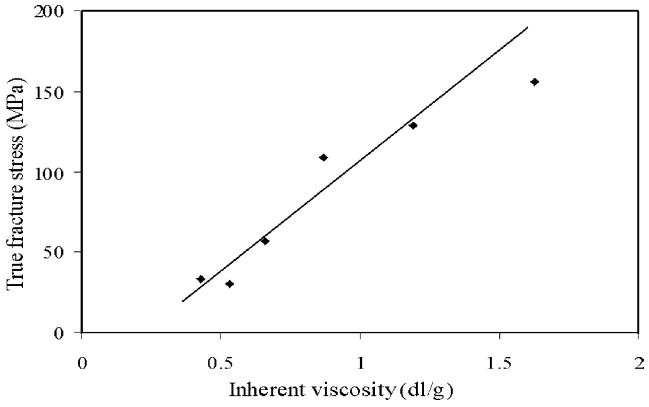


Fig. 10. True fracture stress as function of the inherent viscosity.

The amide segment length of the copolymers ranged from $x = 1$ to 10. With short amide segment length ($x \leq 2$) no phase separation takes place and these short amide segments remain dissolved in the PPO phase. The critical amide segment length at which liquid–liquid demixing takes place was $x_u = 3$. This is close to a critical urethane segment length of 3.3 found for segmented polyurethanes [31].

For the block copolymers ($x > 2$) two transitions were observed indicating the presence of a two-phase morphology. The amide phase as judged from DSC is amorphous, which is in agreement with the irregular structure of the amide. As two amorphous phases are present the phase separation is by liquid–liquid demixing and already taking place in the melt (melt phasing). All the polymers studied ($x > 2$) had spherical amorphous hard domains dispersed in a soft matrix, even at 55 wt% of amide. The size distribution of the liquid–liquid demixed domains is bimodal with nano domains (3–10 nm) and sub-micron domains (30–1000 nm). A bimodal size distribution of domain with similar size scales has been observed before by TEM studies on segmented polyurethanes [32]. The nano-particles are though of containing just amide segments. The larger sub-micron domains cannot consist of

Table 3
Mechanical properties

| Amide segment | Amide length $x_r$ | $\eta_{inh}$ (dl/g) | $G'$ (25 °C) (MPa) | $\sigma_{10\%}$ (MPa) | $\sigma_{break}$ (MPa) | $\varepsilon_{break}$ (%) | $\sigma_{break,true}$[a] (MPa) | TS at 50%[b] (%) |
|---|---|---|---|---|---|---|---|---|
| $I(X_mI)_3$ | 3.3 | 1.62 | 3.7 | 0.35 | 15 | 960 | 160 | 37 |
| $I(X_mI)_4$ | 5.0 | 0.43 | 5.5 | 0.53 | 7.5 | 340 | 35 | – |
| $I(X_mI)5$ | 5.6 | 0.53 | 5.6 | 0.78 | 7.2 | 320 | 30 | 35 |
| $I(X_mI)_6$ | 6.4 | 1.19 | 12 | 2.2 | 18 | 620 | 130 | 25 |
| $I(X_mI)_8$ | 9.3 | 0.87 | 21 | 3.4 | 29 | 270 | 110 | 21 |
| $I(X_mI)_{10}$ | 10.6 | 0.66 | 47 | 3.2 | 20 | 190 | 60 | 19 |

[a] True fracture stress calculated with Eq. (4).
[b] Tensile set at 50% strain.

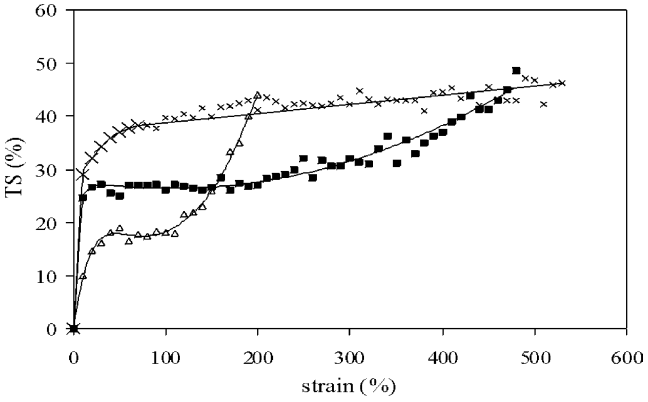


Fig. 11. The tensile set (TS) as function of the applied strain and amide segment length $x_r$: ×, 3.3; ■, 6.4; △, 10.4.

only amide segments, as the amide segments used are short (6–17 nm), but must also contain PPO segments. These domains were found to have a 'salami' morphology. The volume fraction of these larger hard domains is increased with increasing amide segment length.

The storage modulus of these PEEA's increases moderately with increasing particle content and can be described by the Guth–Smallwood relation [24,25]. Still, these PEEA's are soft materials ($G'$ (25 °C) = 1.4–47 MPa and $\sigma_{10\%}$ = 0.35–3.2 MPa) even with amide segment concentrations up to approximately 55 wt%. The fracture properties increase strongly with molecular weight.

The compression and tensile sets values decrease with increasing amide segment length and thus increasing modulus. Probably, the longer amide segments in the hard phase are more resistant to deformation resulting in block copolymers with a higher elasticity. Polymers containing long amide segment length have nano-domains of a larger size and a smaller content and these copolymers were found to have lower compression sets. This may suggest that the nano-domains, and particular small nano-domains, are less resistant to deformation as compared to the sub-micron domains. Giving time (12 days) the compression set of the block copolymers has reduced to 0%. The observed recovery for liquid–liquid demixed PEEA copolymers is a relatively slow process. This viscoelastic process may be due to slow retraction of amide segments being pulled out of the glassy amide domains during deformation.

Increasing the amide segment length in liquid–liquid demixed PEEA copolymers has lead to lower tensile sets in the region of 0–100% applied strain. The tensile set of these polymers increases with strain and levels off after 25% strain. This leveling off of the tensile set is assumed to be due to yielding of the amide phase in the block copolymers. At higher deformations (>100%) another deformation process may be involved as the tensile set increases strongly. When the amide segment length is increased this process starts at lower strains and also becomes more significant.

## Acknowledgements

This research was financed by the Dutch Polymer Institute (DPI, The Netherlands) project number 137. The authors would like to thank Mr Y. Tanabe (Mitsubishi Gas Chemical Co. Inc., Japan) for supplying the *m*-xylylene diamine, and Mr H. Nefzger (Bayer AG, Germany) for supplying the Acclaim™ Polyols. Mr Rico Keim and Mr Mark Smithers (MESA+institute, the Netherlands) are acknowledged for their help and expertise with the TEM-experiments.

## References

[1] Holden G, Legge NR, Schroeder HE, editors. Thermoplastic elastomers: a comprehensive review. 2nd ed. Munich: Hanser Publishers; 1987.
[2] Olabisi O, Robeson LM, Shaw MT, editors. Polymer–polymer miscibility. 1st ed. New York: Academic Press; 1979.
[3] Sperling LH, editor. Introduction to physical polymer science. 3rd ed. New York: Wiley; 2001.
[4] Flory PJ, editor. Principles of polymer chemistry. 1st ed. New York: Cornell University Press; 1953 [chapter 13].
[5] Cella RJJ. J Polym Sci: Symp 1973;42:727.
[6] Phillips RA, Cooper SL. Polymer 1994;35:4146.
[7] Grady BP, Cooper SL. In: Mark JE, Erman B, Eirich FR, editors. Science and technology of rubber. San Diego: Academic Press; 1994 [chapter 13].
[8] Ries G, Hurtez G, Bahadur P. In: Mark HF, Bikales NM, Kroschwitz JI, editors. Encyclopedia of polymer science and engineering, 2nd ed, vol. 2. New York: Wiley; 1985. p. 379–93.
[9] Leibler L. Macromolecules 1980;13:1602.
[10] Hadjichristidis N, Pispas S, Floudos GA, editors. Block copolymers. 1st ed. New Jersey: Wiley; 2003.
[11] Adams RK, Hoeschele GK. In: Holden G, Legge NR, Schroeder HE, editors. Thermoplastic elastomers: a comprehensive review. 1st ed. Munich: Hanser Publishers; 1987 [chapter 8].
[12] Niesten MCEJ, Feijen J, Gaymans RJ. Polymer 2000;(41):8487.
[13] Niesten MCEJ, ten Brinke JW, Gaymans RJ. Polymer 2001;(42): 1461.
[14] Bonart R. Polymer 1979;(20):1389.
[15] Eisenbach CD, Baumgartner M, Gunter G. In: Lal J, Mark JE, editors. Advances in elastomer and rubber elasticity. New York: Plenum Press; 1985.
[16] Elwell MJA, Ryan AJ, Stanford JL. In: Macosko CW, editor. RIM: fundamentals in reaction injection molding. Munich: Carl Hanser Verlag; 1988 [chapter 9].
[17] Broos R, Herrington RM, Casati FM. Cell Polym 2000;(19):169.
[18] Armistead JP, Wilkes GL. J Appl Polym Sci 1988;(35):601.
[19] Kaushiva BD, Wilkes GL. Polymer 2000;(41):6981.
[20] Kaushiva BD, Wilkes GL. Polymer 2000;(41):6987.
[21] Li Y, Desper R, Chu B. Macromolecules 1992;(25):7365.
[22] Koberstein JT, Russel TP. Macromolecules 1986;(19):714.
[23] Tocha E, Janik H, Debowski M, Vancso GJ. J Macrmol Sci-Phys 2002;(B41):1291.
[24] Guth E. J Appl Phys 1945;(16):20.
[25] Smallwood HM. J Appl Phys 1944;(15):758.
[26] Manson JA, Sperling LH, editors. Polymer blends and composites. New York: New Plenum Press; 1976.
[27] Carlston EF, Lum FG. Ind Eng Chem 1957;49:1239.
[28] Van der Schuur JM, Feijen J, Gaymans RJ, *Polymer* in press (Polymer 05-40).
[29] Lothmar J, Meyer K, Goldbach G. Makromol Chem 1988;(189):2053.

[30] Krijgsman J, Husken D, Gaymans RJ. Polymer 2003;(44):7573.
[31] Koberstein JT, Leung LM. Macromolecules 1992;(25):6205.
[32] Neff R, Macosko CW, Ryan AJ. J Appl Polym Sci: Polym Phys 1998; 36:573.
[33] Schierholtz JU, Hellman GP. Polymer 2003;44:2005.
[34] Van Krevelen DW, editor. Properties of polymers. Amsterdam: Elsevier; 1976.
[35] Miller JA, Cooper SL. J Polym Sci: Polym Phys 1985;(23):1065.
[36] Niesten MCEJ, Gaymans RJ. J Appl Polym Sci 2001;(81):1372.
[37] Kausch HH, Béguelin Ph, editors. Encyclopedia of materials: science and technology. Amsterdam: Elsevier Science Ltd; 2001. p. 7399–408.
[38] McCrum NG, Buckley CP, Bucknall CB. Principles of polymer engineering. 2nd ed. New York: Oxford University Press; 2001.